Article

The Kinetic Model of Diffusion and Reactions in Powder Catalysts during Temperature Programmed Oxygen Isotopic Exchange Process

Arvaidas Galdikas [1,2,*], Muhammad Usman [1] and Matas Galdikas [1]

[1]   Physics Department, Kaunas University of Technology, 50 Studentų St., 51368 Kaunas, Lithuania; muhammad.usman@ktu.edu (M.U.); matas.galdikas@ktu.lt (M.G.)
[2]   Department of Physics, Mathematics and Biophysics, Lithuanian University of Health Sciences, 4 Eivenių St., 50166 Kaunas, Lithuania
[*]   Correspondence: arvaidas.galdikas@ktu.lt

Abstract: The mathematical model of diffusion in powder oxide catalysts during the process of temperature programmed oxygen isotopic exchange is proposed. The diffusion is considered together with the homogeneous and heterogeneous oxygen isotopic exchange processes. The matrix forms of exchange rate equations of simple and complex heteroexchange, and homoexchange reactions which obtain symmetrical forms are analyzed. The quantitative values of model parameters are found from the fitting of experimental data taken from literature of temperature programmed oxygen isotopic exchange process in catalysts ZrO_2 and CeO_2. The fittings show a good matching of model results with experimental data. The shapes of kinetic curves registered during temperature programmed oxygen isotopic exchange process are analyzed and the influence of various process parameters such as activation energies of simple and complex heteroexchange, oxygen surface concentration of catalyst, ratio of catalysts surface and volume of reactor, diffusion activation energy is considered. The depth profiles of diffusing oxygen species in oxide catalysts powder are calculated.

Keywords: catalysis; diffusion; modeling; temperature programmed oxygen isotopic exchange; kinetics

1. Introduction

Ceria (CeO_2) and zirconia (ZrO_2) are the main components of the three-way catalysts used in automobile pollutant abatement [1,2]. They enable a control of the partial pressure of oxygen near the catalyst surface during automotive emission [3,4] and are able to store and/or supply oxygen under fuel-lean and fuel-rich conditions, respectively, what is necessary for the conversion of nitrogen oxides, hydrocarbons and carbon monoxide [5,6]. AO_2 (A = Ce,Zr) releases oxygen during rich conditions and is converted to AO_{2-x}, whereas during lean conditions AO_{2-x} is oxidized back to AO_2 [7,8]. These properties are related to the ability of AO_2 system to promote migration/exchange of oxygen species in the reaction [9,10]. Due to high surface and bulk diffusivity, the oxygen atoms can be quickly transferred to the active sites form different parts of the catalysts [11,12]. The highest oxygen storage capacity and catalytic performance of ceria-zirconia materials is at approximately 40–60% of ceria content [13,14].

A powerful tool to study the various oxygen transport processes that may take place in a crystalline oxide is the ^{18}O–^{16}O isotopic exchange technique [15–17]. The oxygen isotopic exchange is a suitable method to analyze the diffusivity and interaction of molecular oxygen with a metal oxide. From the registered kinetic curves of oxygen species concentrations, the mechanisms of catalytic processes and heir rates in given catalyst are determined [18,19]. Three types of exchange mechanisms between gaseous dioxygen and lattice oxygen atom have been defined on oxide catalysts [20,21]: (1) homoexchange between adsorbed atoms itself, without participation of atoms form oxide; (2) simple hetero-exchange between one

atom of adsorbed oxygen molecule and one atom of the solid oxide and (3) the multiple hetero-exchange when both atoms of adsorbed oxygen molecule are exchanged with solid oxide oxygen atoms. Information on the mechanism of exchange may be obtained from the kinetic curves of oxygen species partial pressures at the beginning of exchange reaction. The formation of $^{16}O^{18}O$ species as a primary product from $^{18}O_2$ indicates that exchange takes place via a simple hetero-exchange, if $^{16}O_2$ species are formed firstly, it means multiple hetero-exchange mechanism [22]. Isotopic exchange is generally carried out in a recycle, close reactor coupled to a mass spectrometer [23,24]. The evolution of the partial pressures of $^{16}O_2$, $^{16}O^{18}O$ and $^{18}O_2$ during the exchange process are registered as a function of time in isothermal conditions. When the range of temperatures where the exchange process occurs is not well-known isothermal conditions could turn out to be tedious. In those cases, the method of temperature-programmed oxygen isotopic exchange is very useful. Using a linear and slow increase of sample temperature, the concentration of the adsorbing/reacting/desorbing molecules are registered [25,26]. The curves obtained in one temperature programing isotopic exchange experiment directly inform on the temperature window where the exchange takes place and give a complete view of the proportion of lattice oxygen atoms (surface and bulk) involved in the process depending of the temperature [27]. Such experiment can permit comparison of different families of oxide samples in an easy way, comparing the evolution of the rate of exchange and the evolution of the number of exchanged atoms versus temperature [28]. Increasing the temperature also enables us to rapidly reach an equilibrium between the ^{18}O concentration in the gas phase and into the lattice and then to obtain data about the number of exchangeable atoms in the solid [23].

In the temperature programmed isotopic exchange experiments a very important parameter is the surface area of the catalyst. The high surface area provides more active oxygen transfer from catalyst. In this work the influence of surface is of catalyst is investigated. Oxygen transfer form catalysts goes on through the bulk diffusion processes. The bulk diffusion processes in oxide catalysts where was started to investigate in our previous work Ref. [29]. In this work the complete model of bulk diffusion during and exchange reactions in powder catalysts during temperature programmed oxygen isotopic exchange process is proposed and verification with experimental results is achieved.

2. The Model

Isotopic oxygen exchange on surfaces of catalysts goes on by homoexchange and by heteroexchange [30,31]. Homoexchange occurs without participation of surface oxygen. The heteroexchange takes place when oxygen atoms form the surface of oxide are involved into the process. The simple heteroexchange occurs when one oxygen atom in the molecule is replaced, in complex heteroexchange both oxygen atoms in molecule are replaced [18,22,32]. Simple and complex oxygen isotopic heteroexchange reactions are listed in Table 1.

Table 1. Oxygen exchange reactions. Indexes *g* and *s* means compounds in gas phase and on the surface of oxide. *p* is the probability assuming only those cases when composition is changed.

Simple Heteroexchange Reactions		Complex Heteroexchange Reactions
$^{18}O^{18}O_g + {}^{16}O^{16}O_s \rightarrow {}^{16}O^{18}O_g + {}^{18}O^{16}O_s$	$(p = 1)$	
$^{16}O^{16}O_g + {}^{18}O^{18}O_s \rightarrow {}^{18}O^{16}O_g + {}^{16}O^{18}O_s$	$(p = 1)$	$^{18}O^{18}O_g + {}^{16}O^{16}O_s \rightarrow {}^{16}O^{16}O_g + {}^{18}O^{18}O_s$
$^{16}O^{18}O_g + {}^{16}O^{16}O_s \rightarrow {}^{16}O^{16}O_g + {}^{16}O^{18}O_s$	$(p = 1/2)$	$^{16}O^{16}O_g + {}^{18}O^{18}O_s \rightarrow {}^{18}O^{18}O_g + {}^{16}O^{16}O_s$
$^{16}O^{18}O_g + {}^{18}O^{18}O_s \rightarrow {}^{18}O^{18}O_g + {}^{16}O^{18}O_s$	$(p = 1/2)$	$^{18}O^{18}O_g + {}^{18}O^{16}O_s \rightarrow {}^{18}O^{16}O_g + {}^{18}O^{18}O_s$
$^{18}O^{18}O_g + {}^{18}O^{16}O_s \rightarrow {}^{16}O^{18}O_g + {}^{18}O^{18}O_s$	$(p = 1/2)$	$^{18}O^{16}O_g + {}^{18}O^{18}O_s \rightarrow {}^{18}O^{18}O_g + {}^{18}O^{16}O_s$
$^{16}O^{16}O_g + {}^{18}O^{16}O_s \rightarrow {}^{18}O^{16}O_g + {}^{16}O^{16}O_s$	$(p = 1/2)$	$^{18}O^{16}O_g + {}^{16}O^{16}O_s \rightarrow {}^{16}O^{16}O_g + {}^{18}O^{16}O_s$
$^{18}O^{16}O_g + {}^{16}O^{18}O_s \rightarrow {}^{16}O^{16}O_g + {}^{18}O^{18}O_s$	$(p = 1/4)$	$^{16}O^{16}O_g + {}^{18}O^{16}O_s \rightarrow {}^{18}O^{16}O_g + {}^{16}O^{16}O_s$
$^{16}O^{18}O_g + {}^{18}O^{16}O_s \rightarrow {}^{18}O^{18}O_g + {}^{16}O^{16}O_s$	$(p = 1/4)$	

Not all of the simple hetero-exchange reactions listed in Table 1 result in a change in system composition. It may happen that an atom of the same type from the gas phase can be replaced with an atom of the same type from the surface (e.g., $^{16}O_g$ with $^{16}O_s$). In that case microscopically the oxygen exchange occurs, but the composition of system remains the same. In order to involve into the calculation only those cases of reaction which lead to compositional changes of system, in Table 1 for simple heteroexchange reactions the probabilities are indicated. Through the probabilities that are included only those cases of exchange when composition of system occurs. Considering adsorption, in the proposed model it is assumed that adsorption is very fast process [33,34] and surface is covered by oxygen species with the same composition as composition in gas phase. The change in composition in the gas phase and on the surface is calculated according to the law of mass action well known in chemistry. Using this law in the case of simple heteroexchange the variation of concentrations in gas phase n_{32}, n_{34} and n_{36} of species $^{16}O^{16}O_g$, $^{16}O^{18}O_g$ and $^{18}O^{18}O_g$, respectively, expressed in mol/m^3 is written as follows:

$$\left(\tfrac{dn_{32}}{dt}\right)_S = k_S\left(-\left(c_{36}+\tfrac{1}{2}c_{34}\right)n_{32} + \tfrac{1}{2}\left(c_{32}+\tfrac{1}{2}c_{34}\right)n_{34}\right)$$
$$\left(\tfrac{dn_{34}}{dt}\right)_S = k_S\left(\left(c_{36}+\tfrac{1}{2}c_{34}\right)n_{32} - \tfrac{1}{2}(c_{32}+c_{34}+c_{36})n_{34} + \left(c_{32}+\tfrac{1}{2}c_{34}\right)n_{36}\right) \qquad (1)$$
$$\left(\tfrac{dn_{36}}{dt}\right)_S = k_S\left(\tfrac{1}{2}\left(c_{36}+\tfrac{1}{2}c_{34}\right)n_{34} - \left(c_{32}+\tfrac{1}{2}c_{34}\right)n_{36}\right)$$

where: k_S is the rate constant of simple heteroexchange reactions and is expressed by Arrhenius law: $k_S = A_S exp(-Q_S/RT)$, where A_S and Q_S are pre-exponential term and activation energy of simple heteroexchange. R and T are gas constant and temperature, respectively. The variables c_{32}, c_{34} and c_{36} are surface concentrations of species adsorbed on the surface $^{16}O^{16}O_S$, $^{16}O^{18}O_S$ and $^{18}O^{18}O_S$, respectively, expressed in mol/m^2. The variation of surface concentration c_{32}, c_{34} and c_{36} are found from following relation:

$$\left(\tfrac{dc_{32}}{dt}\right)_S = \tfrac{V}{S}k_S\left(\tfrac{1}{2}c_{34}n_{32} + \tfrac{1}{2}\left(-c_{32}+\tfrac{1}{2}c_{34}\right)n_{34} - c_{32}n_{36}\right)$$
$$\left(\tfrac{dc_{34}}{dt}\right)_S = \tfrac{V}{S}\left(\tfrac{dn_{34}}{dt}\right)_S \qquad (2)$$
$$\left(\tfrac{dc_{36}}{dt}\right)_S = \tfrac{V}{S}k_S\left(-c_{36}n_{32} + \tfrac{1}{2}\left(-c_{36}+\tfrac{1}{2}c_{34}\right)n_{34} + \tfrac{1}{2}c_{34}n_{36}\right)$$

where V is volume of reactor and S is surface area of catalyst. Only equation for c_{32} is symmetrical to equation for n_{34}. Ratio V/S appears because of different dimensions of concentrations in gas phase n_{ij} expressed in mol/m^3 and surface concentrations c_{ij} expressed in mol/m^2. Later it will be shown that this ratio, which seems to be just technical parameter in fact plays very important role.

Using law of mass action in the case of complex heteroexchange the variation of concentrations in gas phase is written as follows:

$$\left(\tfrac{dn_{32}}{dt}\right)_C = k_C\left(-(c_{36}+c_{34})n_{32} + c_{32}n_{34} + c_{32}n_{36}\right)$$
$$\left(\tfrac{dn_{34}}{dt}\right)_C = k_C\left(c_{34}n_{32} - (c_{32}+c_{36})n_{34} + c_{34}n_{36}\right) \qquad (3)$$
$$\left(\tfrac{dn_{34}}{dt}\right)_C = k_C\left(c_{36}n_{32} + c_{36}n_{34} - (c_{32}+c_{34})n_{36}\right)$$

where k_C is reaction rate constant of complex heteroexchange expressed by Arrhenius law $k_C = A_C exp(-Q_C/RT)$, where A_C and Q_C are pre-exponential term and activation energy of complex heteroexchange. Due to the symmetry of complex heteroexchange reactions (that is not the case for simple heteroexchange), the variations of variables c_{32}, c_{34} and c_{36} can be written in very simple form.

$$\left(\frac{dc_i}{dt}\right)_C = \frac{V}{S}\left(\frac{dn_i}{dt}\right)_C, \quad i = 32, 34, 36 \qquad (4)$$

From the mathematical point of view, it is very interesting to analyze obtained sets of Equations (1)–(3). For example, the Equation (3) keeping n_{32}, n_{34} and n_{35} as variables can be written in the following matrix.

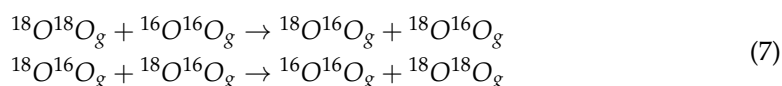$$\begin{pmatrix} -(c_{36}+c_{34}) & c_{32} & c_{32} \\ c_{34} & -(c_{32}+c_{36}) & c_{34} \\ c_{36} & c_{36} & -(c_{32}+c_{34}) \end{pmatrix} \tag{5}$$

The Equation (5) is symmetrical in various cross sections and show interesting mathematical regularities of system where the complex heteroexchange of isotopes takes place. For simple heteroexchange the Equation (1) obtains the following matrix form.

$$\begin{pmatrix} -\left(c_{36}+\frac{1}{2}c_{34}\right) & \frac{1}{2}\left(c_{32}+\frac{1}{2}c_{34}\right) & 0 \\ \left(c_{36}+\frac{1}{2}c_{34}\right) & \frac{1}{2}(c_{32}+c_{34}+c_{36}) & \left(c_{32}+\frac{1}{2}c_{34}\right) \\ 0 & \frac{1}{2}\left(c_{36}+\frac{1}{2}c_{34}\right) & -\left(c_{32}+\frac{1}{2}c_{34}\right) \end{pmatrix} \tag{6}$$

Equation (6) also is symmetric in various cross sections and show mathematical regularities in complex heteroexchange systems. More detail and deep analysis of those matrixes could give very useful additional information about the properties of the system.

In the case of homoexchange, when exchange occurs only between adsorbed molecules without participation of lattice atoms the reactions in which the change of system composition takes place are following [20,21].

$$^{18}O^{18}O_g + {}^{16}O^{16}O_g \rightarrow {}^{18}O^{16}O_g + {}^{18}O^{16}O_g$$
$$^{18}O^{16}O_g + {}^{18}O^{16}O_g \rightarrow {}^{16}O^{16}O_g + {}^{18}O^{18}O_g \tag{7}$$

The rate equations mathematically describing those reactions applying the mass action law are the next:

$$\left(\frac{dn_{32}}{dt}\right)_O = k_O\left(n_{34}^2 - n_{32}n_{36}\right)$$
$$\left(\frac{dn_{34}}{dt}\right)_O = 2k_O\left(-n_{34}^2 + n_{32}n_{36}\right) \tag{8}$$
$$\left(\frac{dn_{36}}{dt}\right)_O = k_O\left(n_{34}^2 - n_{32}n_{36}\right)$$

where k_O is rate constant of homoexchange expressed by Arrhenius law as $k_o = A_o exp(-Q_o/RT)$, A_O and Q_O are preexponential term and activation energy of homoexchange, respectively. In the case of molar concentrations of n_{ij} dimension of k_O is m^4/s mol.

Similar to Equations (5) and (6), if writing Equation (8) in matrix form keeping n_{32}, n_{34} and n_{35} as variables the following two equivalent matrixes can be written

$$\begin{pmatrix} 0 & n_{34} & -n_{32} \\ 0 & -2n_{34} & 2n_{32} \\ 0 & n_{34} & -n_{32} \end{pmatrix} \text{ or } \begin{pmatrix} -n_{36} & n_{34} & 0 \\ 2n_{36} & -2n_{34} & 0 \\ -n_{36} & n_{34} & 0 \end{pmatrix} \tag{9}$$

Considering the process of bulk diffusion, when oxygen isotope atoms ^{18}O penetrate in deeper layers of oxide, the concentration variation of oxygen atoms in one oxide layer *K* as given is calculated by using the second Fick's law expressed in finite increments. However, first it must be adapted to geometrical specifics of particles of powder catalysts. The particles of ceria and zirconia powder catalysts, which experimental results will be fitted by proposed model, have cubic-like geometrical form [35,36]. Describing mathematically the process of diffusion into bulk of powder particle it is necessary to assume the limitation of the depth. The Fick's law expressed in finite increments means that the bulk is deleted into separate layers but in the cases of powder particles, when diffusion flux takes place from for all surfaces into the center of powder particle the area of layers decreases. To solve this problem, the cubic-like powder particles are virtually divided into four pyra-

mids and in 2-d case each of them is divided into layers (see Figure 1). The area of each K layer can be found form the following relation:

$$S_B^{(K)} = S_{ox}\left(1 - 2(K-1)\frac{h}{d_{ox}}\right)^2 \tag{10}$$

where S_{ox} is the area of surface layer, h is the thickness of layer and d_{ox} is the size of powder particle. The second Fick's law expressed in finite increments, assuming decreasing areas of layers obtains the following form:

$$\left(\frac{dc_i^{(L,K)}}{dt}\right)_{SD} = \frac{D}{h^2}\left(B^{(K-1)}\left(c_i^{(L,K-1)} - c_i^{(L,K-1)}\right) - B^{(K)}\left(c_i^{(L,K)} - c_i^{(L,K+1)}\right)\right), \ K > 1 \tag{11}$$

where D is the bulk diffusion coefficient of oxygen atoms in oxide, $i = 16, 18$ indicates the type of oxygen isotopes and coefficients $B^{(K)}$ involve the changes of areas of layers and are expressed as:

$$B^{(K)} = \begin{cases} \frac{S^{(K+1)}}{S^{(K)}} & , if \ c_i^{(L,K)} - c_i^{(L,K+1)} \geq 0 \\ \frac{S^{(K)}}{S^{(K+1)}} & , if \ c_i^{(L,K)} - c_i^{(L,K+1)} < 0, \end{cases} \tag{12}$$

It is assumed that diffusion of oxygen isotopes are balanced, i.e., ^{18}O diffuses into the bulk and replaces ^{16}O atoms which diffuses to the surface and the condition $\left(dc_{18}^{(K)}/dt\right)_{dif} = -\left(dc_{16}^{(K)}/dt\right)_{dif}$ is fulfilled. Diffusion coefficient of both oxygen species is assumed the same.
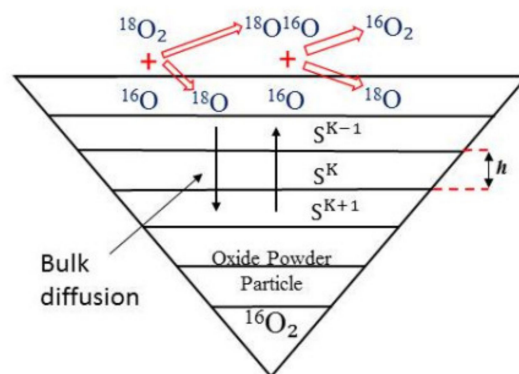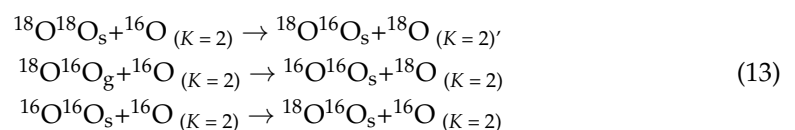

Figure 1. Scheme of the layers introduced for bulk diffusion calculations in particle of powder catalyst.

As indicated in Equation (11) $K > 1$ the equation describes diffusion starting from the second layer $K \geq 2$, $K = 1$ is the surface, first or adsorption layer where oxygen species form gas phase adsorbs (and desorbs). The equation is needed which could describe diffusion and oxygen exchange between surface (first) layer and second layer of catalysts. The mass action law in combination with Fick's law we will use to build equation for diffusion between first and second monolayers.

The exchange reactions between oxygen species on the surface $^{18}O^{18}O$, $^{16}O^{18}O$ and $^{16}O^{16}O$ with oxygen atoms from second monolayer ^{16}O $_{(K=2)}$ and ^{18}O $_{(K=2)}$ are considered [29]:

$$\begin{aligned} ^{18}O^{18}O_s + {}^{16}O \ _{(K=2)} &\rightarrow {}^{18}O^{16}O_s + {}^{18}O \ _{(K=2)'} \\ ^{18}O^{16}O_g + {}^{16}O \ _{(K=2)} &\rightarrow {}^{16}O^{16}O_s + {}^{18}O \ _{(K=2)} \\ ^{16}O^{16}O_s + {}^{16}O \ _{(K=2)} &\rightarrow {}^{18}O^{16}O_s + {}^{16}O \ _{(K=2)} \end{aligned} \tag{13}$$

Using the mass action law and taking into account the gradient of concentrations the reaction rates of those reaction are expressed in following form:

$$\left(\frac{dn_{32}}{dt}\right)_{dif} = \frac{D}{h^2}k_d\left(c_{18}^{(1)} - c_{18}^{(2)}\right)\left(\frac{1}{2}c_{34} - c_{32}\right)c_{16}^{(2)}$$

$$\left(\frac{dn_{34}}{dt}\right)_{dif} = \frac{D}{h^2}k_d\left(c_{18}^{(1)} - c_{18}^{(2)}\right)\left(c_{36} + c_{32} - \frac{1}{2}c_{34}\right)c_{16}^{(2)} \qquad (14)$$

$$\left(\frac{dn_{36}}{dt}\right)_{dif} = \frac{D}{h^2}k_d\left(c_{18}^{(1)} - c_{18}^{(2)}\right)c_{34}c_{16}^{(2)}$$

where k_d is the reaction rate constant, $c_{16}^{(1)}$ and $c_{18}^{(1)}$ are atomic concentrations of oxygen of ^{16}O and ^{18}O on the surface $K = 1$ and are calculated form concentrations of molecular species $^{16}O^{16}O$, $^{16}O^{18}O$ and $^{18}O^{18}O$ from the next relation:

$$c_{16}^{(1)} = c_{32} + \frac{1}{2}c_{34}$$

$$c_{18}^{(1)} = c_{36} + \frac{1}{2}c_{34} \qquad (15)$$

Finally, the kinetics of composition in gas phase is calculated including all considered above processes simple and complex heteroexchange, homoexchange and diffusion:

$$\frac{dn_i}{dt} = \left(\frac{dn_i}{dt}\right)_S + \left(\frac{dn_i}{dt}\right)_C + \left(\frac{dn_i}{dt}\right)_O + \left(\frac{dn_i}{dt}\right)_{dif}, \; i = 32, 34, 36 \qquad (16)$$

The temperature programming exchange.

In the model the reaction rate constants k_S, k_C, k_O, k_d and diffusion coefficient D depend on temperature according to Arrhenius law $k_j = A_j exp\left(-Q_j/RT(t)\right)$, A_O and Q_O are preexponential term and activation energy of. In temperature programming exchange process the temperature T depends on time linearly: $T(t) = T_0 + bt$, where T_0 is initial temperature and b the rate temperature increase, t is the time.

3. Results and Discussion

In Figure 2a,b the experimental and calculated dependencies of partial pressures of oxygen species $^{18}O_2$, $^{18}O^{16}O$ and $^{16}O_2$ on temperature are presented. Results are calculated for ZrO_2 and CeO_2. Experimental results are taken form literature Refs. [35,36]. The temperature programmed oxygen isotopic exchange experiment was performed at following conditions: the temperature increase speed 1.6 °C/min, specific surface area $S_{bet} = 25$ m^2/g for ceria and $S_{bet} = 25$ m^2/g for zirconia, mass of powder catalyst $m_{cat} = 0.25$ g, initial pressure of $^{18}O_2$ 48 mbar and volume of reactor $V = 12$ cm^3. The surface concentration of oxygen in ceria depending on crystallite orientation varies from 0.97 nm^2 for (110) until 15.8 nm^2 for (111) [35,36] and in these calculations was taken as 1.09×10^{19} m^2. Similarly using data from Ref. [36] for zirconia oxygen surface concentration was taken 1.09×10^{19} m^{-2}. From the fitting of experimental curves presented in Figure 2, the values of activation energies of simple and complex heteroexchange reactions, diffusion and its pre-exponential terms were found. Values are written in Table 2.

The fitting results presented in Figure 2 are quite good, taking into account the difficulty of the process. In TPIE experiments the temperature changes with time and curves in Figure 2 represent not a simple dependency on temperature but the kinetic curves. Some deviations of calculated results form experimental ones in many cases occurs because of impurities, which always exist in real conditions and which are impossible to estimate in modeling. For zirconia Figure 2a some deviation of calculated curves form experimental points occurs considering the temperature range where the process of exchange starts. Experimental results show that exchange process starts at a little lower temperatures tha, theoretical predictions. However, for ceria catalysts Figure 2b the calculated curves very well correspond with experimental points in this interval of temperatures. For ceria a small deviation is observed at higher temperatures when steady state of process is reached,

but only for p_{34} curve, the curve p_{32} show very good agreement in whole considered temperature interval. Comparing the temperature interval where the exchange process starts the lower temperature is for ceria catalyst.
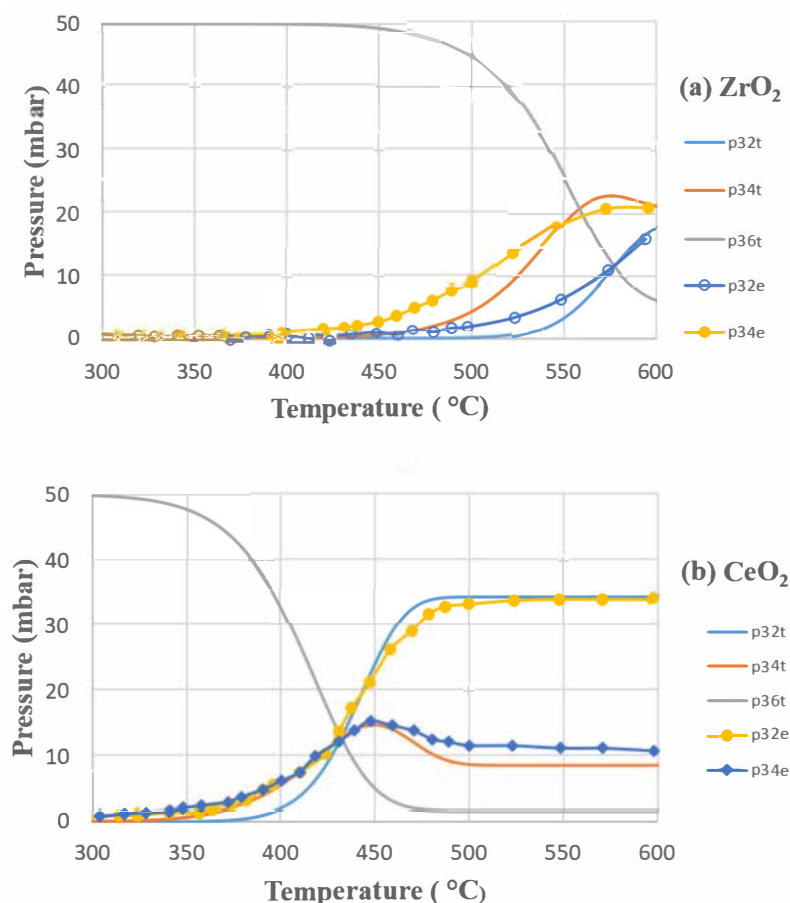

Figure 2. Calculated (lines) and experimental (points+line) [35,36] dependencies of partial pressures of oxygen species on temperature for catalyst ZrO_2 (**a**) and CeO_2 (**b**) during TPIE.

Table 2. Values of calculation parameters of Figure 2.

Parameters	Ceria	Zirconia
A_C	3.6×10^{-8} m^2 s^{-1}	4.0×10^{-8} m^2 s^{-1}
A_S	0.96×10^{-11} m^2 s^{-1}	1.0×10^{-11} m^2 s^{-1}
A_{dif}	1.58×10^{-24} m^2 s^{-1}	1.90×10^{-24} m^2 s^{-1}
Q_C	176 kJ·mol^{-1}	180 kJ·mol^{-1}
Q_S	118 kJ·mol^{-1}	120 kJ·mol^{-1}
Q_{dif}	135 kJ·mol^{-1}	154 kJ·mol^{-1}

Measuring composition changes in gas phase during TPIE process the important parameter is the ratio between volume of reactor and total surface of catalyst V/S which is involved into calculations through Equations (2) and (4). This ratio influences significantly the partial pressures of oxygen species, including the steady state regime. This ratio depends on mass of catalysts and specific surface area through the relation $S = m_{cat} \cdot S_{bet}$. This relation also means that the same influence in the kinetic curves have both parameters mass of catalyst and specific area of catalyst. Moreover, because in Equations (2) and (4) the ratio V/S exist, the volume of catalyst also significantly affects the shapes kinetic curves and the values of partial pressures when steady state is reached. At the steady

state if when mass of catalysts is relatively high $p_{34} < p_{32}$ and when catalyst mass is low, situation is in opposite: $p_{34} > p_{32}$. However, it is important to consider the influence of process parameters on the shapes of kinetic curves and partial pressures of species at steady state regime.

In Figure 3 the calculated curves of partial pressures of oxygen species at steady state regime as a dependency on ratio S/V are presented. The shapes of curves p_{34} and p_{32} significantly differs. The curve p_{34} pass maximum while the curve p_{32} goes up in whole interval of S/V. The position of maximum in curve p_{34} corresponds with position of cross section point of pressure curves of p_{32} and p_{36}. The curves p_{32} and p_{34} cross each other and after the amount of species $^{16}O_2$ at steady state becomes higher than $^{18}O^{16}O$ with further increase of S/V. The point at which curves p_{32} and p_{34} cross each other depends on total pressure: it shifts to lower values of S/V when total pressure decreases. It is seen in Figure 2 (dot lines).
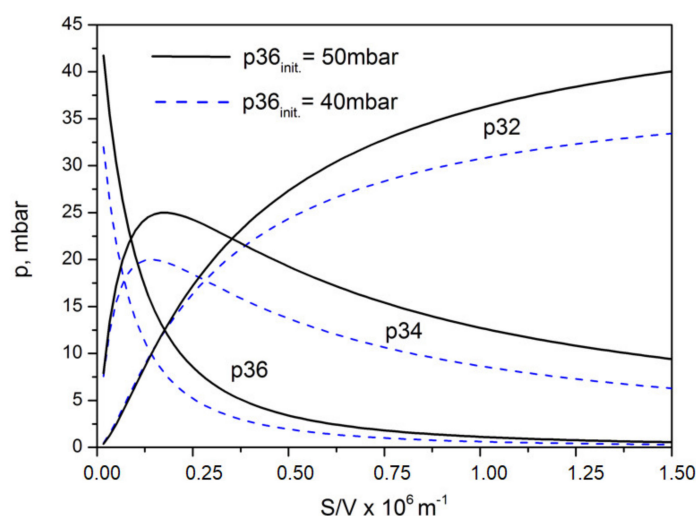

Figure 3. Calculated dependencies of partial pressures of oxygen species at steady state regime on ratio S/V.

Experimental kinetic curves of oxygen species partial pressures registered during TPIE may have quite different shapes. For example, the curve p_{34} in Figure 2b has a maximum, but the curve p_{34} not. Many experimental results show that the maximums can be broad or narrow, high or low, or sometimes they are not formed at all. It depends on type of catalyst. In order to clarify this situation and to find some regularities the calculations were performed by varying activation energies of simple and complex heteroexchange. The influence of Q_S and Q_C (activation energies of simple and complex exchange) is analyzed in Figure 4a the calculated curves obtained by changing Q_C and (b) the curves by changing Q_S are presented. From Figure 4a it is seen that with increase of Q_C the temperature at which the molecules $^{16}O_2$ start to form shifts to higher temperatures and this shift at the beginning is very significant and later reduces (see 4 and 5 curves). However, the temperature of formation of $^{16}O^{18}O$ species almost does not depend on Q_C but the shape of p_{34} curves significantly depends on Q_C. At low values of Q_C the maximum is not observed in those curves, but it appears and increases with the increase of Q_C. In opposite it is for p_{32} curves, at low Q_C the broad but not well-expressed maximum is seen but with increase of Q_C it disappears. The influence of Q_S which presented in Figure 4b is different. The temperature of formation of $^{16}O^{18}O$ species is very sensitive on Q_S and it is not so sensitive for formation of $^{16}O_2$ molecules, especially at higher values of Q_S (see 4 and 5 curves of p_{32}). Maximums in p_{34} curves are well expressed at lower values of Q_S and disappear at high values of Q_S. In opposite it is for p_{32} curves, no maximums are seen at low values of Q_S and broad maximums appear at high values of Q_S. From Figure 4a,b it is seen that Q_S and Q_C values determine which oxygen species

with increase of temperature will be formed first. Depending on Q_S and Q_C values with increase of temperature the oxygen species $^{16}O^{18}O$ can start to form first and $^{16}O_2$ after or in opposite, $^{16}O_2$ first and $^{16}O^{18}O$ after. The cases when both oxygen species start to form together at the same temperature also can be observed in Figure 4.

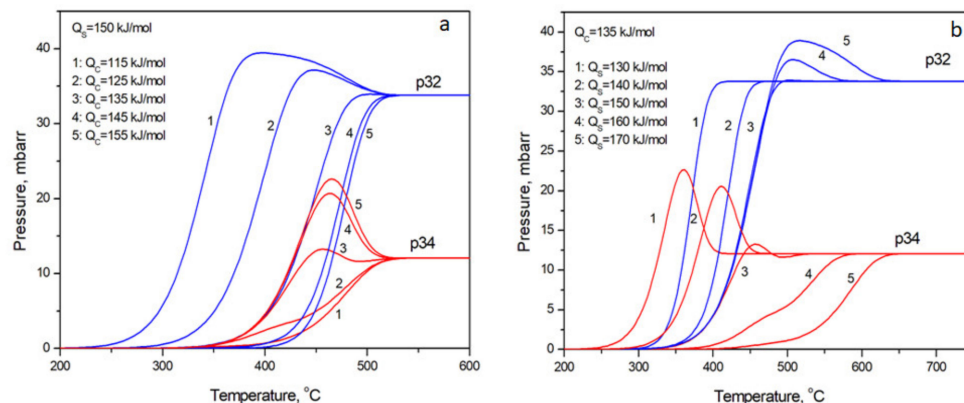**Figure 4.** Calculated dependencies of partial pressures of oxygen species on temperature for the case of steady state pressures $p_{32} > p_{34}$: (**a**) influences of Q_C and (**b**) Q_S.

The results presented in Figure 4 were obtained at relatively high ratio of S/V, in the case when steady state pressures as $p_{32} > p_{34}$. The case of relatively low ratio S/V when steady state pressures are $p_{32} < p_{34}$ is considered in Figure 5. In Figure 5a the influence of Q_C is shown. It is seen that curves of p_{34} almost are not affected by changes of Q_C, but curves p_{32} are significantly affected by Q_C. At low values of Q_C curves p_{32} have big and broad maximums which decrease and finally disappear with increase of Q_C. In Figure 5a it is also seen that at low values of Q_C with increase of temperature species of $^{16}O_2$ are formed firstly and $^{16}O^{18}O$ after. However, the situation reversely changes at high values of Q_C: $^{16}O^{18}O$ are formed first and then $^{16}O_2$. The influence of Q_C in the case when steady state pressures fulfil condition $p_{32} < p_{34}$ is presented in Figure 5b. Now, the change of Q_S significantly affects both curves. At higher values of Q_S the maximums in curves p_{32} start to appear and become broader with increase of Q_S. However, it is interesting to note that when maximum appears, the temperature of formation of $^{16}O_2$ does not change any more with further increase of Q_S. The curves of p_{34} continuously shift to higher temperatures with increase of Q_S but the shape of curves remain the same and no maximums appear. At low values of Q_S with increase of temperature the species of $^{16}O^{18}O$ are formed firstly and then $^{16}O_2$, but at high values of Q_S situation reversely changes: species $^{16}O_2$ first and $^{16}O^{18}O$ after.
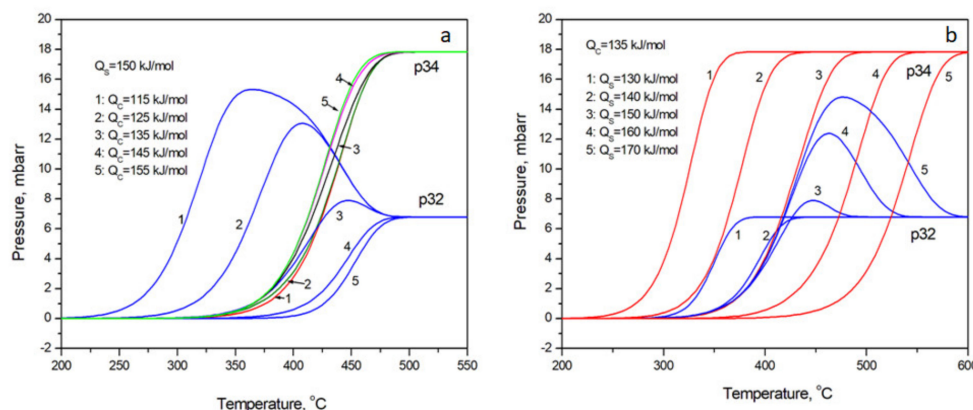

Figure 5. Calculated dependencies of partial pressures of oxygen species on temperature for the case of steady state pressures $p_{32} < p_{34}$: (**a**) influences of Q_C and (**b**) Q_S.

Considering the steady state pressures of oxygen species, it is important to note that additionally to ratio *S/V*, there is another parameter which influences the steady state pressures and modifies the kinetic. This parameter is the initial surface concentration of oxygen C_{OX}. In the model this parameter is involved through the initial value of surface concentration c_{32}. Parameter c_{32} is variable but at the beginning at $t = 0$ it equals to C_{OX}: c_{32} $(t = 0) = C_{OX}$. Surface concentration of oxygen depends on the type of catalyst, method of preparation and also orientation of oxide crystallite grains [35,36]. The influence of oxygen surface concentration is shown in Figure 6 where the partial pressure curves calculated for different surface concentration of oxygen C_{OX} are presented. It is seen that in contrast with curves presented in Figures 4 and 5, the curves of Figure 6 at steady state regime differs. Since C_{OX} depends on crystallite surface orientation curves presented in Figure 6 can also be considered as presentation of the influence of crystallite surface orientation catalysts. Parameter C_{OX} affects both, the temperature of formation of oxygen species and the pressure at steady state regime.
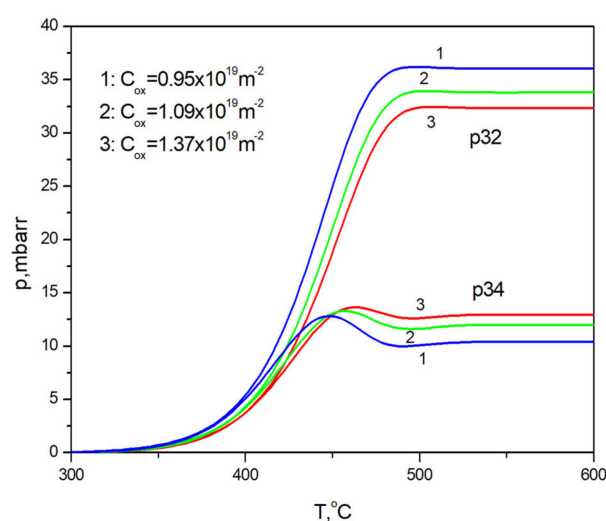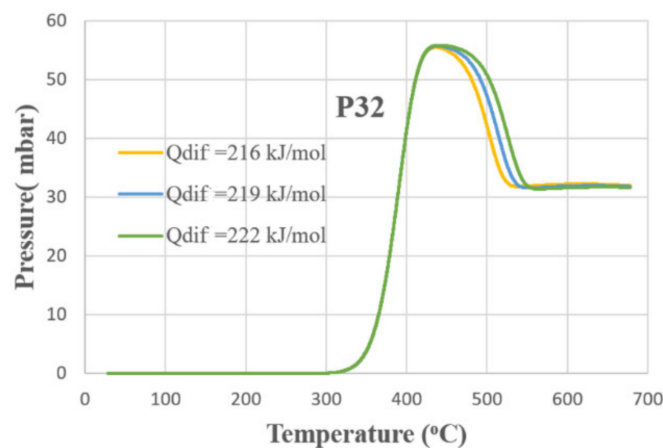

Figure 6. Calculated dependencies of partial pressures of oxygen species on temperature for different values of concentration of oxygen on the surfaces of oxides.

In the heterogeneous exchange, the process of diffusion is very important and influences the kinetic curves. The influence of bulk diffusion process is shown in Figure 7 where the calculated kinetic curves of partial pressure of oxygen specie $^{16}O_2$ as a dependency on temperature (which increases with time in TPIE) are presented. The curves are calculated at different values of diffusion activation energy at constant pre-exponential factor $A_{dif} = 1.90 \cdot 10^{-24}$ m^{2}s^{-1}. All other parameters were kept as constants and were the same as in calculations presented in in Figure 2b. It is seen that diffusion significantly influences the shape of kinetic curves in the transition period and at steady state. The partial pressure at steady state of $^{16}O_2$ decreases with increase of Q_{dif}. This result is logic, because the increase of Q_{dif} means the decrease of diffusivity. At higher diffusivity more amount of $^{16}O_2$ appear in gas phase because of diffusion of oxygen atoms from the bulk of catalyst. In order to see this effect in more detail the dependence of $^{16}O_2$ partial pressure at steady state regime is presented in Figure 8. The considered interval is narrow and change of pressure is small, nevertheless, the nonlinear dependence of steady state partial pressure on diffusivity can be seen.

In order to check the validity of model the concentration distribution in deeper layers, the concentration deps profiles of atoms ^{16}O and ^{18}O were calculated. Results are presented in Figure 9, where depth profile curves are calculated for different values of Q_{dif}. Obtained curves are typical diffusion curves and shows the correctness of calculations. However, the bulk diffusion on powder catalysts is not so simple as discussed above presenting Figure 1 and Equation (12) and depth profile curves at higher diffusivity can be more

complex. It is seen that with increase of diffusivity (decrease of Q_{dif}) the concentration of ^{16}O at the surface layers decreases and is replaced by oxygen ^{18}O coming from gas phase. It means what more oxygen ^{16}O must appear in gas phase forming oxygen species $^{16}O_2$ and $^{16}O^{18}O$.

Figure 7. Calculated dependencies of partial pressures of oxygen species on temperature for different values of concentration of oxygen on the surfaces of diffusion activation energies Q_{dif}.
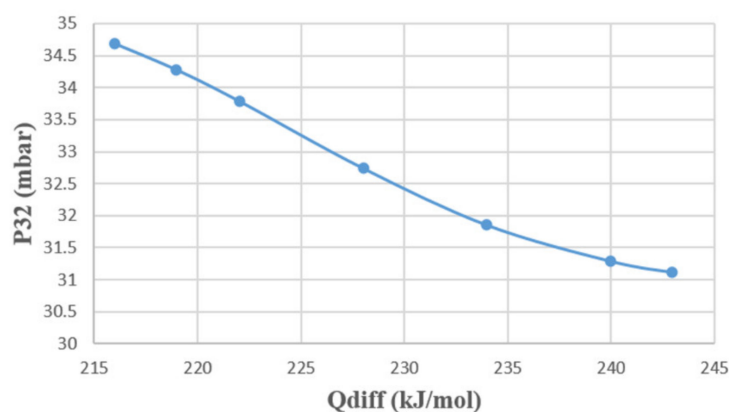
Figure 8. The dependence of pressure at steady state regime on Q_{dif}.
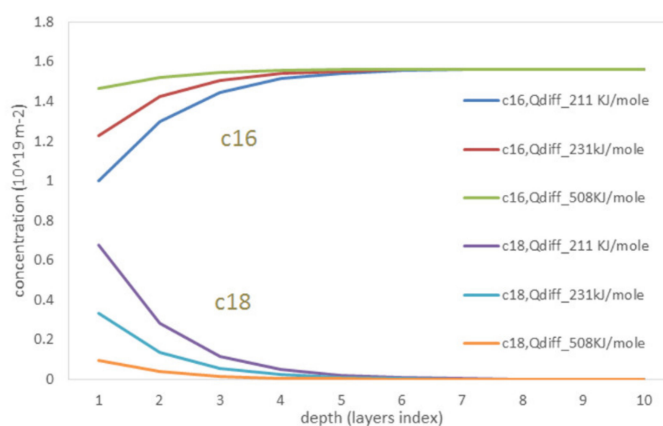
Figure 9. The depth profiles of oxygen atoms calculated at different values of Q_{dif}.

Above the bulk diffusion was considered, but the surface diffusion is also very important in catalysis. It depends on homogeneity of surface. In the case of homogeneous surface, the exchange takes place directly on surface of oxide, the surface diffusion does not change

surface composition of species and mathematically there is no need to write new equation because of absence of new variables. Concentration gradients on the surface in that case are not formed and it is not possible to consider surface mobility of atoms. Situation is significantly different in the case of nonhomogeneous surfaces, e.g., when noble metal nanoparticles are formed on the surfaces of oxides such as in M/CeO_2 (M-noble metal, e.g., Pt, Pd, Au) catalysts. Such catalysts are used in order to reduce oxygen exchange temperature [23] (which on noble metals is less) what is very important in automotive catalysts. In that case, because of spillover [12,37,38] the oxygen concentration gradients are formed toward metal nanoparticles. The model of surface and bulk diffusion because of oxygen spillover was proposed in our previous works [33,34]. In these studies the surface diffusion was combined with bulk diffusion and finally two dimensional diffusion model was created for consideration of nonhomogeneous catalysts such as $M/Ce_xZr_{(1-x)}O_2$. It was found [28,39] that process of bulk diffusion becomes more important with increase of content of Zr. For pure ceria CeO_2 samples bulk diffusion is weak and dominates surface diffusion.

4. Conclusions

1. The matrix forms of equations of simple and complex isotopic heteroexchange have symmetry in various cross sections and show interesting mathematical regularities.
2. Despite the variety of different shapes of partial pressure kinetic curves registered during TPIE there are strict regularities: (a) in the case of $p_{34} < p_{32}$ at steady state, the p_{34} curves have well expressed maximums or may be without extremums at higher values of activation energies or together with maximum can exist minimum; the p_{32} curves approaches steady state passing broad maximums or without them but never through the minimums. (b) in the case $p_{34} > p_{32}$ at steady state, the p_{32} curve approaches steady state passing broad maximums or without them at higher activation energies, p_{34} curve approaches steady state without extremums.
3. The main parameter determining the steady state partial pressures of oxygen species is the ratio of catalyst specific surface area to volume of reactor. Surface atomic concentration bulk diffusion also influences state partial pressures. Steady state partial pressures are not influenced by reaction rates of heteroexchange.
4. The bulk diffusion process significantly influences the shapes of kinetic curves and partial pressures of species at steady state regime.

References

1. Teschner, D.; Wootsch, A.; Röder, T.; Matusek, K.; Paál, Z. Ceria as a new support of noble metal catalysts for hydrocarbon reactions: Chemisorption and catalytic studies. *Solid State Ion.* **2001**, *141*, 709–713. [CrossRef]
2. Moschovi, A.; Giuliano, M.; Kourtelesis, M.; Nicol, G.; Polyzou, E.; Parussa, F.; Yakoumis, I.; Sgroi, M. First of its kind automotive catalyst prepared by recycled PGMs-catalytic performance. *Catalysts* **2021**, *11*, 942. [CrossRef]
3. Nelson, A.E.; Schulz, K.H. Surface chemistry and microstructural analysis of $Ce_xZr_{1-x}O_{2-y}$ model catalyst surfaces. *Appl. Surf. Sci.* **2003**, *210*, 206–221. [CrossRef]
4. Machida, M.; Fujiwara, A.; Yoshida, H.; Ohyama, J.; Asakura, H.; Hosokawa, S.; Tanaka, T.; Haneda, M.; Tomita, A.; Miki, T.; et al. Deactivation mechanism of $Pd/CeO_2–ZrO_2$ three-way catalysts analyzed by chassis-dynamometer tests and in situ diffuse reflectance spectroscopy. *ACS Catal.* **2019**, *9*, 6415–6424. [CrossRef]
5. Jen, H.W.; Graham, G.W.; Chun, W.; McCabe, R.W.; Cuif, J.P.; Deutsch, S.E.; Touret, O. Characterization of model automotive exhaust catalysts: Pd on ceria and ceria–zirconia supports. *Catal. Today* **1999**, *50*, 309–328. [CrossRef]
6. Gong, J.; Wang, D.; Li, J.; Kamasamudram, K.; Currier, N.; Yezerets, A. An experimental and kinetic modeling study of aging impact on surface and subsurface oxygen storage in three-way catalysts. *Catal. Today* **2019**, *320*, 51–60. [CrossRef]
7. Suhonen, S.; Valden, M.; Hietikko, M.; Laitinen, R.; Savimäki, A.; Härkönen, M. Effect of Ce–Zr mixed oxides on the chemical state of Rh in alumina supported automotive exhaust catalysts studied by XPS and XRD. *Appl. Catal. A-Gen.* **2001**, *218*, 151–160. [CrossRef]
8. Rafaj, Z.; Krutel, J.; Nehasil, V. Oxygen exchange between catalyst and active support during CO oxidation on $Rh/CeO_2(111)$ and $Rh/CeO_2(110)$: Isotope labeled ^{18}O study. *J. Phys. Chem. C* **2021**, *125*, 15959–15966. [CrossRef]
9. Kašpar, J.; Fornasiero, P.; Graziani, M. Use of CeO_2-based oxides in the three-way catalysis. *Catal. Today* **1999**, *50*, 285–298. [CrossRef]
10. Nakanishi, Y.; Suehiro, Y.; Hashimoto, M.; Narishige, T. Development of Low Temperature Active Three Way Catalyst. SAE Technical Paper 2019-01-1293. 2019. Available online: https://doi.org/10.4271/2019-01-1293 (accessed on 10 May 2021).
11. Ojala, S.; Bion, N.; Gomes, S.R.; Keiski, R.L.; Duprez, D. Isotopic oxygen exchange over Pd/Al_2O_3 catalyst: Study on $C^{18}O_2$ and $^{18}O_2$ exchange. *ChemCatChem* **2010**, *2*, 527–533. [CrossRef]
12. Rajbala; Bhatia, D. Crystallite-scale approach to predict the oxygen storage capacity of a three-way catalyst for natural gas applications. *Ind. Eng. Chem. Res.* **2019**, *58*, 10271–10284. [CrossRef]
13. Rood, S.; Eslava, S.; Manigrasso, A.; Bannister, C. Recent advances in gasoline three-way catalyst formulation: A review. *Proc. Inst. Mech. Eng. Part J. Automob. Eng.* **2020**, *234*, 936–949. [CrossRef]
14. Hajar, Y.M.; Boreave, A.; Caravaca, A.; Vernoux, P.; Baranova, E.A. Isotopic oxygen exchange study to unravel noble metal oxide/support interactions: The case of RuO_2 and IrO_2 nanoparticles supported on CeO_2, TiO_2 and YSZ. *ChemCatChem* **2020**, *12*, 2548–2555. [CrossRef]
15. Bouwmeester, H.J.M.; Song, C.; Zhu, J.; Yi, J.; Annaland, M.V.S.; Boukamp, B.A. A novel pulse isotopic exchange technique for rapid determination of the oxygen surface exchange rate of oxide ion conductors. *Phys. Chem. Chem. Phys.* **2009**, *11*, 9640–9643. [CrossRef] [PubMed]
16. MacQueen, B.; Ruiz-Yi, B.; Royko, M.; Heyden, A.; Pagan-Torres, Y.; Williams, C.T.; Lauterbach, J.A. In-situ oxygen isotopic exchange vibrational spectroscopy of rhenium oxide surface structures on cerium oxide. *J. Phys. Chem. C* **2020**, *124*, 7174–7181. [CrossRef]
17. Winter, L.R.; Chen, R.; Chen, X. Elucidating the roles of metallic Ni and oxygen vacancies in CO_2 hydrogenation over Ni/CeO_2 using isotope exchange and in situ measurements. *Appl. Catal. B Environ.* **2019**, *245*, 360–366. [CrossRef]
18. Doornkamp, C.; Clement, M.; Ponec, V. The isotopic exchange reaction of oxygen on metal oxides. *J. Catal.* **1999**, *182*, 390–399. [CrossRef]
19. Dong, F.; Tanabe, T.; Takahashi, N.; Shinjoh, H. Investigation of the effective oxygen storage and release performances on the Pt/CeO_2-ZrO_2 catalysts by breakthrough method. *Catal. Today* **2019**, *332*, 259–266. [CrossRef]
20. Klier, K.; Nováková, J.; Jíru, P. Exchange reactions of oxygen between oxygen molecules and solid oxides. *J. Catal.* **1963**, *2*, 479–484. [CrossRef]
21. Novakova, J. Isotopic exchange of oxygen ^{18}O between the gaseous phase and oxide catalysts. *Catal. Rev.* **1971**, *4*, 77–113. [CrossRef]
22. Descorme, C.; Madier, Y.; Duprez, D. Infrared study of oxygen adsorption and activation on cerium–zirconium mixed oxides. *J. Catal.* **2000**, *196*, 167–173. [CrossRef]
23. Sadykov, V.; Eremeev, N.; Sadovskaya, E.; Bobin, A.; Ishchenko, A.; Pelipenko, V.; Muzykantov, V.; Krieger, T.; Amanbaeva, D. Oxygen mobility and surface reactivity of $PrNi_{1-x}Co_xO_{3-\delta}$ perovskites and their nanocomposites with $Ce_{0.9}Y_{0.1}O_{2-\delta}$ by temperature-programmed isotope exchange experiments. *Solid State Ion.* **2015**, *273*, 35–40. [CrossRef]
24. Penkala, B.; Aubert, D.; Kaper, H.; Tardivat, C.; Conder, K.; Paulus, W. The role of lattice oxygen in CO oxidation over $Ce^{18}O_2$-based catalysts revealed under operando conditions. *Catal. Sci. Technol.* **2015**, *5*, 4839–4848. [CrossRef]
25. Boaro, M.; Vicario, M.; de Leitenburg, C.; Dolcetti, G.; Trovarelli, A. The use of temperature-programmed and dynamic/transient methods in catalysis: Characterization of ceria-based, model three-way catalysts. *Catal. Today* **2003**, *77*, 407–417. [CrossRef]
26. Marinho, A.L.A.; Rabelo-Neto, R.C.; Epron, F.; Bion, N.; Toniolo, F.S.; Noronha, F.B. Embedded Ni nanoparticles in CeZrO2 as stable catalyst for dry reforming of methane. *Appl. Catal. B Environ.* **2020**, *268*, 118387. [CrossRef]

27. Liang, Q.; Wu, X.; Wu, X.; Weng, D. Role of surface area in oxygen storage capacity of ceria-zirconia as soot combustion catalyst. *Catal. Lett.* **2007**, *119*, 265–270. [CrossRef]

28. Duprez, D. Study of surface reaction mechanisms by 16O/18O and H/D isotopic exchange. *Catal. Today* **2006**, *112*, 17–22. [CrossRef]

29. Galdikas, A.; Bion, N.; Duprez, D.; Virbickas, V.; Mazelis, D. Modeling of diffusion process in the isotopic oxygen exchange experiments of CexZr(1−x)O2 catalysts. *Mater. Sci.* **2013**, *19*, 83–88. [CrossRef]

30. Den Otter, M.W.; Boukamp, B.A.; Bouwmeester, H.J.M. Theory of oxygen isotope exchange. *Solid State Ion.* **2001**, *139*, 89–94. [CrossRef]

31. Farlenkov, A.S.; Khodimchuk, A.V.; Eremin, V.A.; Tropin, E.S.; Fetisov, A.V.; Shevyrev, N.A.; Leonidov, I.I.; Ananyev, M.V. Oxygen isotope exchange in doped lanthanum zirconates. *J. Solid State Chem.* **2018**, *268*, 45–54. [CrossRef]

32. Sadovskaya, E.M.; Ivanova, Y.A.; Pinaeva, L.G.; Grasso, G.; Kuznetsova, T.G.; van Veen, A.; Sadykov, V.A.; Mirodatos, C. Kinetics of oxygen exchange over CeO_2-ZrO_2 fluorite-based catalysts. *J. Phys. Chem. A* **2007**, *111*, 4498–4505. [CrossRef] [PubMed]

33. Galdikas, A.; Descorme, C.; Duprez, D. Surface diffusion upon oxygen isotopic exchange on oxide-supported metal nanoclusters. *Solid State Ion.* **2004**, *166*, 147–155. [CrossRef]

34. Galdikas, A.; Descorme, C.; Duprez, D.; Dong, F.; Shinjoh, H. Study of the oxygen diffusion on three-way catalysts: A kinetic model. *Top. Catal.* **2004**, *30*, 405–409. [CrossRef]

35. Madier, Y.; Descorme, C.; Le Govic, A.M.; Duprez, D. Oxygen mobility in CeO_2 and $Ce_xZr_{(1-x)}O_2$ compounds: Study by CO transient oxidation and $^{18}O/^{16}O$ isotopic exchange. *J. Phys. Chem. B* **1999**, *103*, 10999–11006. [CrossRef]

36. Madier, Y. Etude de la Mobilité et du Stockage de l'Oxygène par Echange Isotopique 18O/16O sur des Catalyseurs de Postcombustion à Base d'Oxydes de Terres Rares. Ph.D. Thesis, Poitiers University, Poitiers, Fance, 1999.

37. Henry, C.R. Catalytic activity of supported nanometer-sized metal clusters. *Appl. Surf. Sci.* **2000**, *164*, 252–259. [CrossRef]

38. Ananyev, M.V.; Porotnikova, N.M.; Eremin, V.A.; Kurumchin, E.K. Interaction of O_2 with LSM–YSZ composite materials and oxygen spillover effect. *ACS Catal.* **2021**, *11*, 4247–4262. [CrossRef]

39. Bedrane, S.; Descorme, C.; Duprez, D. Investigation of the oxygen storage process on ceria- and ceria-zirconia-supported catalysts. *Catal. Today* **2002**, *75*, 401–405. [CrossRef]